ELSEVIER

Applied Surface Science 202 (2002) 160–182

applied surface science

www.elsevier.com/locate/apsusc

Atomistic simulations of surface coverage effects in anisotropic wet chemical etching of crystalline silicon

M.A. Gosálvez*, A.S. Foster[1], R.M. Nieminen

Laboratory of Physics, Helsinki University of Technology, 02015 Espoo, Finland

Received 02 April 2002; accepted 31 July 2002

Abstract

Atomistic simulations of anisotropic wet chemical etching of crystalline silicon have been performed in order to determine the dependence of the etch rates of different crystallographic orientations on surface coverage and clustering of OH radicals. We show that the etch rate is a non-monotonic function of OH coverage and that there always exists a coverage value at which the etch rate reaches a maximum. The dependence of the anisotropy of the etching process on coverage, including the dependence of the fastest-etched plane orientation, is implicitly contained in the model and predictions of convex corner under-etching structures are made. We show that the whole etching process is controlled by only a few surface configurations involving a particular type of next-nearest neighbours. The relative value of the removal probabilities of these configurations determines the balance in the occurrence of step propagation and etch pitting for all surface orientations.

PACS: 81.65.Cf; 82.65.-i

Keywords: Anisotropic wet chemical etching; Cellular Automaton; Surface coverage; Surface termination; Surface morphology; Mask; Convex corner; Silicon

1. Introduction

Anisotropic wet chemical etching of silicon in alkaline solutions [1] is one of the key techniques for the manufacture of microsystems. However, the microscopic mechanisms responsible for the strong anisotropy are still debated. Allongue et al. [2,3] and Allongue [4] have proposed that the process is a combination of chemical and electrochemical reaction routes. As a consequence, the amount of anisotropy observed macroscopically is explained by the relative occurrence of the two reactions under the specific etching conditions of each experiment. Hydroxyl ions OH^- from the etching solution play a central role. They substitute the surface-terminating hydrogens and catalyse the removal of the surface atoms by weakening their backbonds [4]. However, it has been shown recently [5] that these surface substitutions are considerably restricted at certain surface configurations. This is due to the existence of significant interaction between the terminating hydroxyl and the terminating species at the next-nearest neighbours, H or OH. Actually, the existence of these restrictions explains the appearance of high-index fastest-etched planes, a major feature of the anisotropy observed in the etching

* Corresponding author. Tel.: +358-9-451-3114.
E-mail addresses: mag@fyslab.hut.fi (M.A. Gosálvez), asf@fyslab.hut.fi (A.S. Foster).
[1] Co-corresponding author.

0169-4332/02/$ – see front matter
PII: S0169-4332(02)00903-0

patterns. Notably, these results have been obtained by considering the *average interaction* between the two terminating groups (H and OH). In the present work, we study the effects of the H/OH and OH/OH interactions by explicitly considering the amount of surface coverage by each of the species. This enables us to explain the non-monotonic dependence of the etch rates on concentration and to understand the essential microscopic mechanisms responsible for the strong anisotropy of the etching process.

1.1. Surface coverage

During the etching process, the surface of silicon can be both hydrogen and hydroxyl-terminated, depending on the concentration and pH value of the etchant [6]. Even in the case of H dominance, OH groups still terminate a significant fraction of the surface sites [4], providing the mechanism for further etching. Due to the weakening effect that the OH terminations have on the backbonds [5], the evolution of the etching process is expected to be strongly correlated to the amount of OH coverage. However, this correlation need not be linear for the complete range of surface coverage, since the weakening of backbonds is not the only mechanism involved in the process. The geometrical restrictions to the attachment of OH groups must also be taken into account. In this way, a non-monotonic dependence of the etch rate on coverage is expected for any crystallographic orientation. As the coverage increases, the etching process becomes faster, since more and more OH groups provide larger amounts of weaker bonds, which are more susceptible for thermal breaking. However, as the OH coverage is increased further, the existence of significant OH/OH interactions between the increasing number of terminating hydroxyls eventually slows down the etching process. Since the process which destroys hydroxyl (hydrogen) terminations produces hydrogen (hydroxyl) terminations [6], the etch rate should become vanishingly small for the limiting cases of complete hydrogen and complete hydroxyl termination (complete passivation). Therefore, we conclude that, for any crystallographic orientation, there should exist a value of coverage at which the etch rate reaches a maximum. One of the purposes of this work is to show that, in spite of the simplicity of the previous reasoning, the existence of a maximum in the etch rates as a function of coverage (or concentration) is more subtle than expected and requires the incorporation of the effects from next-nearest neighbours of nearest neighbours.

1.2. Clustering

According to Allongue [4], the rate-limiting step for the formation of a solvable Si complex is the first substitution of a terminating hydrogen by a hydroxyl group. After this substitution, the sequence of further chemical steps is fast [4]. Therefore, it can be expected that OH termination of the neighbouring atoms of initially OH-terminated sites will occur shortly after the initial first substitution, before detachment of the solvable Si complex. In fact, there is experimental evidence [7] indicating the existence of OH *clustering* at the initially OH-terminated sites in an otherwise 'fully' H-terminated surface. It is therefore important to establish to what extent the existence of clustering affects the etch rates and the anisotropy of the etching process in general.

We will refer by *clustering* to the subsequent substitutions (of H by OH), *induced* by one initial substitution at a particular target atom, taking place both at the target atom itself (if it is initially terminated by more than one H) and at the first neighbours (if they are H-terminated). Induced substitutions occurring at neighbours located further away than the first neighbours are not considered. Their coverage state (either H or OH, for each of the dangling bonds) is determined by the nominal value of the surface coverage and is assumed to be uncorrelated to the initial substitution which induces the clustering process. Within this framework, we will refer to *maximal clustering* as the complete OH termination of the dangling bonds of the target atom and all its first neighbours, allowing the second and further neighbours to be partly or totally OH-terminated or H-terminated.

2. Atomistic simulations

In order to study the effects of OH coverage and clustering on the etching process, we carry out atomistic simulations using a Cellular Automaton (CA) approach. We note that similar atomistic simulations can also be realised using a kinetic Monte Carlo approach [5,8]. A detailed comparison of the performance of

both methods for the simulation of anisotropic wet chemical etching can be found in [9].

Generally speaking, in atomistic simulations the atoms of the surface are visited one by one and their neighbourhoods are inspected in order to determine the probability of removal of the atom and decide whether the atom is removed or remains attached. The probability of removal is related to the state of the neighbourhood because it determines not only the number of backbonds (which need to be broken in order to remove the atom) but also their energy. The number of bonds is fixed by the number of first neighbours, and their energy is determined by the number of OH groups attached to the surface atom and to its first neighbours [5,10].

Usually, the criterion used in these models in order to remove the surface atoms is simple: removal occurs if a random number is smaller than the removal probability corresponding to the current configuration of the neighbourhood. Otherwise, the surface atom remains attached. In the CA approach, all the surface atoms are first visited in order to decide on their removal according to this criterion. Then, all those surface atoms for which removal has been found are removed at once and the state of their neighbourhoods is updated. The time evolution of the whole surface is obtained as this type of complete surface updates are consecutively generated.

Since the evolution of each surface atom is controlled by the previous removal criterion (which involves the comparison of two numbers) the method can be considered to be *discrete*. Alternatively, it is possible to define a *Continuous* Cellular Automaton (CCA) [11]. In this approach, a continuous variable ranging from 1 to 0 is used to characterise the 'mass' of each atom in the system. For each visited surface atom, this continuous variable is reduced by an amount corresponding to the removal probability, even if the removal trial was not successful. Then, when the 'mass' of the atom reaches the minimum value of zero, the atom is removed. In this way, more macroscopic features of the etching process can be studied since minor random microscopic fluctuations of the system (due to the implicit stochastic nature of the discrete removal criterion) are eliminated.

In this work, we report on atomistic simulations using the CCA scheme. The algorithm used is developed from a discrete Monte Carlo scheme [8,9].

3. Microscopic model

The anisotropy of wet chemical etching is the result of two microscopic mechanisms [5]: the weakening of backbonds following OH termination of surface atoms and the existence of significant interaction between these hydroxyl groups and other species (such as hydrogen and other hydroxyl groups) terminating the next-nearest neighbours.

3.1. Ab initio energetics

We have carried out electronic structure calculations in order to clarify how bond weakening occurs. The ab initio calculations were performed with the Amsterdam Density Functional (ADF) code [12], implementing the density functional theory (DFT) using the gradient-corrected BLYP functional [13,14]. The code uses Slater-type basis functions and all atoms calculated are represented by triple-zeta basis sets with two polarisation functions, with frozen inner orbitals. Atoms are relaxed to minimise total energy and atomic forces using a conjugate gradient algorithm.

To model the hydrogen/hydroxyl covered silicon surface we consider an H-terminated (Si_{18}) cluster with adsorbed hydroxyl groups at various different sites. This cluster is produced by taking a section out of the (1 0 0) silicon surface, freezing the two bottom layers at the experimental geometry and then fully relaxing the remaining atoms. Table 1 shows that calculated vibrational frequencies for Si–H, O–H and Si–O bonds in this cluster show excellent agreement with previous surface/cluster calculations and experimental surface values, demonstrating the suitability of the cluster model for representing surface processes. Note that the calculated Si–H frequency from [15] in Table 1 has been scaled directly to the

Table 1
Comparison of theoretical and experimental vibrational frequencies for different bonds in silicon

Bond	ν (cm^{-1})		
	Calculated (this study)	Calculated [15,16]	Experimental [15,17]
Si–H	2098	2084	2084
O–H	3734	3596	3680
Si–O	843	876	820

experimental value to serve as a reference for other frequencies in that work, and it is included for completeness.

In order to calculate the bond-breaking energies for different surface environments we use 10 different cluster configurations, where each cluster has from zero to two hydroxyl groups adsorbed on the top three Si atoms. After calculating the relaxed total energy for the cluster configuration, the apex atom (and any H and/or OH bonded to it) is separated from the rest of the cluster. The relaxed total energy is then re-calculated with the separated Si frozen. The difference between the normal and separated total energy for one configuration provides the bond-breaking energy for a specific set of bonds, and by combining the results from all 10 configurations a complete atom removal energy hierarchy is produced.

The calculations show that the weakening of backbonds depends only on the total number of hydroxyls attached to both atoms sharing the bond. In this way, the energy of a bond between two atoms, one terminated by i OH groups and the other terminated by j groups (an 'i–j bond', where $i,j = 0,1,2,3$) can be written as:

$$\epsilon_{ij} = \epsilon_0 - (i+j)\epsilon, \tag{1}$$

where ϵ_0 is the bond energy between two bulk atoms ($\epsilon_0 \approx 2.7$ eV) and ϵ is the energy by which each bond is weakened for every OH group attached to either atom ($\epsilon \approx 0.4$ eV). For instance, this means that the energy cost of breaking a 1–1 bond is the same as for a 2–0 bond. Note that, for any two atoms on the surface, the configurations 0–0 and 3–3 will never occur since the former describes a bond between two bulk atoms and the latter a free molecule not linked to the rest of the system.

The total energy corresponding to the backbonds of a surface atom can be calculated using the matrix ϵ_{ij}. For instance, for the case of a target atom having n first neighbours, each of which has itself n_j first neighbours ($j = 1,2,\ldots,n$; $n_j = 1,2,3,4$), the total energy of the n backbonds will be:

$$E = \sum_{j=1}^{n} \epsilon_{(4-n),(4-n_j)}. \tag{2}$$

Here we have assumed conditions of *maximal clustering*, i.e. complete OH termination of the dangling bonds of the target atom and the first neighbours, although second and further neighbours can also be H-terminated, depending on the nominal coverage of the surface. Note that under this condition, $4-n$ OH groups are attached to the target atom and $4-n_j$ are attached to neighbour j. For more complicated termination situations in which both H and OH terminate the target atom and its first neighbours, similar expressions can be written. In the most general case, the target atom will be terminated by m OH groups, where $m \leqslant 4-n$, and the jth first neighbour will be terminated by m_j OH groups, where $m_j \leqslant 4-n_j$. Then the total energy corresponding to the backbonds will be:

$$E = \sum_{j=1}^{n} \epsilon_{m,m_j}. \tag{3}$$

3.2. Indirect second neighbours

The other microscopic mechanism playing a major role in wet chemical etching, namely, the existence of significant interaction between the terminating hydroxyl groups, and hydrogen and/or other hydroxyl groups, depends only on the presence of *indirect second neighbours* [5]. These are next-nearest neighbours which cannot be reached from the target atom by a covalent-bond path passing directly through a first neighbour. Thus, if a covalent-bond link is to be established, an *indirect* (longer) path along the bonding structure of the crystal has to be followed. On the contrary, a *direct* second neighbour is linked to the target atom by a covalent path *directly* passing through a first neighbour. As an example, second neighbours C1 through C6 in Fig. 1(a) are *direct* and second neighbours C7 and C8 are *indirect*.

The presence of an indirect second neighbour imposes additional geometrical restrictions on the hydroxyl substitution of the hydrogen terminating the dangling bond oriented towards the indirect second neighbour, reducing in effect the probability of OH termination as compared to the case where no indirect second neighbour is present. This is ultimately due to the extra interaction between the hydroxyl group (which substitutes the terminating hydrogen) and a hydrogen atom or a hydroxyl group that terminates the indirect neighbour. This geometrical restriction is especially significant if the target atom has either two or

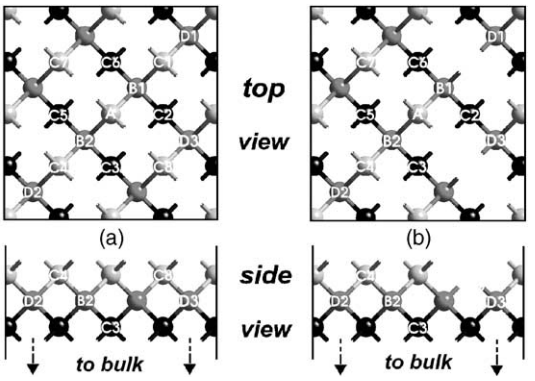

Fig. 1. (a) Target atom A represents a typical atom of an ideal (1 0 0) surface. It has two first neighbours (B1, B2) and eight second neighbours (C1–C8). C1 through C6 are typical *direct* second neighbours, because they are linked to A by a covalent path through B1/B2. However, C7 and C8 cannot be linked to A by the corresponding covalent paths, because the first neighbours are missing. (b) The neighbourhood of atom A has now only six second neighbours (C2–C7). Note that D1 restricts the attachment of a hydroxyl onto B1 in the same manner as C7 does it for A.

three first neighbours, because the rigidity of the bond configuration in both cases prevents any major relaxation mechanism from providing full minimisation of the interaction between the terminating species. However, when the target atom has only one first neighbour, the restrictions in geometry can be overcome, because the atom can rotate about the direction of the bond and, in effect, cancel out the interaction between the terminating species.

So far we have considered the effect of the geometrical restrictions on the termination probability of the target atom only. However, it becomes apparent that also the hydroxyl terminations of the first neighbours (which weaken the backbonds of the target atom in just the same way as the hydroxyl terminations of the target atom itself) suffer from the same type of geometrical restrictions. In this case, however, these are imposed by the next-nearest neighbours of the first neighbours themselves. As an example, Fig. 1(b) shows how atom D1 (an indirect second neighbour of B1, a first neighbour of the target atom A) restricts the attachment of OH groups onto B1 just in the same way as C7 does it for the target atom A. Also note that D1 is located further away from A than a typical third neighbour (such as D3). Since both the target atom (TA) and the first neighbours (FN) can have indirect second neighbours (ISN) affecting their OH termination probabilities, we will denote the indirect second neighbours *of the first neighbours* (such as D1) by $\mathrm{ISN_{FN}}$ and the indirect second neighbours *of the target atom* (such as C7) by $\mathrm{ISN_{TA}}$.

It can be anticipated that no extra effects from further neighbours should be expected, since, according to Eq. (3), the *energy of the backbonds* of the target atom depends only on the OH termination state of the target atom and the first neighbours, but not on the termination state of further neighbours.

The major effects of the geometrical restrictions (namely, the appearance of high-index fastest-etched planes [5]) are observed already even if the $\mathrm{ISN_{FN}}$ are not incorporated and an *average* of the H/OH and OH/OH interactions is used. By explicitly considering any surface coverage conditions by H and OH, we will show in the present study that a physically meaningful behaviour of the etch rate of any crystallographic plane as a function of the surface coverage conditions requires the incorporation of the effects from the $\mathrm{ISN_{FN}}$.

3.3. Removal probabilities

In order to use the previous model in atomistic simulations, the two microscopic mechanisms described must be incorporated into the expression for the probability of removal of the atoms. We write down the removal probability in terms of the Boltzmann factor

$$p = \mathrm{e}^{-\Delta E/k_\mathrm{B}T}, \tag{4}$$

and define the *energy excess* ΔE as:

$$\Delta E = k_\mathrm{B}T \ln\left[1 + \mathrm{e}^{(E-E_\mathrm{c}^A)/k_\mathrm{B}T}\right]. \tag{5}$$

Fig. 2(a) shows the qualitative behaviour of the excess energy. At $T = 0$, $\Delta E = \max(0, E - E_\mathrm{c}^A)$. However, at finite temperature the curve departs from the linear behaviour in the region around $E = E_\mathrm{c}^A$. From the sketch of p in Fig. 2(b) we may regard E_c^A as a *critical energy* (at $T = 0$), acting at finite T as a blurry threshold below which the removal of the atom occurs with probability $p \approx 1$.

The total energy E appearing in the definition of ΔE contains the contribution from the backbonds (as, e.g. in Eq. (2)) and, if indirect second neighbours are present, the contribution from the interactions between the terminating species. Thus, we need to

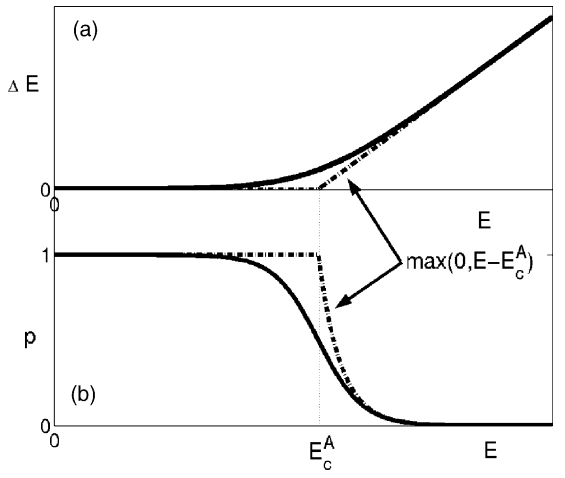

Fig. 2. Qualitative behaviour of the energy excess ΔE and the removal probability p.

define the energies involved in this case. Let us first consider the $\mathrm{ISN_{TA}}$ such as C7 and C8 in Fig. 1(a). Let $e^{\mathrm{TA}}_{\mathrm{OH,OH}}$ refer to the energy of the interaction between two hydroxyls, one terminating the target atom and the other terminating the indirect second neighbour. Similarly, let $e^{\mathrm{TA}}_{\mathrm{OH,H}}$ refer to the energy of the interaction between a hydroxyl and a hydrogen, the former terminating the target atom and the latter terminating the indirect second neighbour. Note that the reverse configuration (i.e. H attached to the target atom) would have the same interaction energy. However, the configuration does not contribute to the energy of removal of the target atom because the attachment of zero hydroxyls to TA should cost nothing. Since the interaction between two hydrogens does not contribute any additional energy either, and the two cases of interest contain always at least one OH group, we will simplify the notation as: $e^{\mathrm{TA}}_{\mathrm{OH}} \equiv e^{\mathrm{TA}}_{\mathrm{OH,OH}}$ and $e^{\mathrm{TA}}_{\mathrm{H}} \equiv e^{\mathrm{TA}}_{\mathrm{OH,H}}$.

In a similar way, for the case of the $\mathrm{ISN_{FN}}$ such as D1 in Fig. 1(b), we will denote by $e^{\mathrm{FN}}_{\mathrm{OH}}$ the energy of the interaction between two hydroxyls, and by $e^{\mathrm{FN}}_{\mathrm{H}}$ the energy of the interaction between one hydroxyl and one hydrogen, the former attached to the first neighbour and the latter attached to the indirect second neighbour.

Let us consider again the particular case of *maximal clustering* (Section 1.2). Consider a target atom with n first neighbours and with $l^{\mathrm{OH}}_{\mathrm{TA}}$ ($l^{\mathrm{H}}_{\mathrm{TA}}$) indirect second neighbours terminated by OH (H). Consider also that each of the n first neighbours has itself n_j first neighbours ($j = 1, 2, \ldots, n$; $n_j = 1, 2, 3, 4$) and $l^{\mathrm{OH}}_{\mathrm{FN},j}$ ($l^{\mathrm{H}}_{\mathrm{FN},j}$) indirect second neighbours terminated by OH (H). Then, the total energy E of the atom is given by:

$$E = \sum_{j=1}^{n} \epsilon_{(4-n),(4-n_j)} + (l^{\mathrm{OH}}_{\mathrm{TA}}\, e^{\mathrm{TA}}_{\mathrm{OH}} + l^{\mathrm{H}}_{\mathrm{TA}}\, e^{\mathrm{TA}}_{\mathrm{H}})(1 - \delta_{1n}) + \sum_{j=1}^{n} (l^{\mathrm{OH}}_{\mathrm{FN},j}\, e^{\mathrm{FN}}_{\mathrm{OH}} + l^{\mathrm{H}}_{\mathrm{FN},j}\, e^{\mathrm{FN}}_{\mathrm{H}})(1 - \delta_{1n_j}). \quad (6)$$

Here, the first term makes use of the energy matrix ϵ_{ij} in order to determine the total energy corresponding to the n backbonds (Eq. (2)). The second term incorporates the effect from the $\mathrm{ISN_{TA}}$, and the third term incorporates the same effect for the $\mathrm{ISN_{FN}}$. The symbol δ_{ij} is the 'Kronecker delta' ($\delta_{ij} = 1$ if $i = j$ and $\delta_{ij} = 0$ if $i \neq j$) and is used in order to add the indirect neighbour term only in the case that the number of first neighbours is 2 or 3, as described in Section 3.2. This is done both for the target atom itself (second term) and for each of its first neighbours (third term).

For more general termination situations in which both H and OH terminate the target atom and its first neighbours, the expressions for the second and third terms of E become more elaborate. However, the idea is still simple: add the energies $e^{\mathrm{TA}}_{\mathrm{OH}}$, $e^{\mathrm{TA}}_{\mathrm{H}}$, $e^{\mathrm{FN}}_{\mathrm{OH}}$ and $e^{\mathrm{FN}}_{\mathrm{H}}$ whenever the corresponding configurations are present. Thus, we will not attempt to write the form of those terms explicitly.

3.4. Biased clustering

According to Section 3.2, it would seem that $e^{\mathrm{TA}}_{\mathrm{OH}} = e^{\mathrm{FN}}_{\mathrm{OH}}$ and $e^{\mathrm{TA}}_{\mathrm{H}} = e^{\mathrm{FN}}_{\mathrm{H}}$. However, by allowing for differences between these interaction energies, the relative importance of the $\mathrm{ISN_{TA}}$ and the $\mathrm{ISN_{FN}}$ for *the removal of the target atom* can be stressed. Moreover, other clustering configurations than *maximal clustering* can be studied qualitatively using the maximal clustering expression for E (Eq. (6)). For instance, by taking $e^{\mathrm{FN}}_{\mathrm{OH}} < e^{\mathrm{TA}}_{\mathrm{OH}}$ and $e^{\mathrm{FN}}_{\mathrm{H}} < e^{\mathrm{TA}}_{\mathrm{H}}$ the contribution to the energy from any $\mathrm{ISN_{FN}}$ will be smaller than for any $\mathrm{ISN_{TA}}$. In a scenario where both the target atom and its first neighbours are assumed to be completely OH-terminated (maximal clustering), this means that the total energy contribution from the attachment of OH to the first neighbours is less than would correspond to the assumed complete OH termination of the first neighbours. This is equivalent to a

configuration with incomplete OH termination of the first neighbours involving higher interaction energies for e_{OH}^{FN} and e_{H}^{FN} (i.e. e_{OH}^{TA} and e_{H}^{TA}, respectively), which thus represents a situation of *biased clustering* towards the target atom. Therefore, the different interaction energies can be used to describe other clustering situations than maximal clustering without actually creating them. The idea resembles that of [5], where a particular value of the average energy of the H/OH and OH/OH interactions was used to represent a particular (although unknown) coverage of the surface.

Following the previous discussion, we use the following relations for all the results presented in this work:

$$e_{OH}^{FN} = e_{OH}^{TA} - 0.2\,\text{eV}, \tag{7}$$

$$e_{H}^{FN} = e_{H}^{TA} - 0.2\,\text{eV}. \tag{8}$$

The subtraction of 0.2 eV is made keeping in mind that, according to the ab initio calculations [5], the value of the H/OH interaction energy e_{H}^{TA} is 0.2 eV. In this way, $e_{H}^{FN} = 0.0$ eV. Thus, we have shifted the zero of the interaction energy from the H/H interaction to the H/OH interaction at ISN_{FN}. For the case of *maximal clustering*, this choice represents complete OH termination of the target atom but incomplete for the first neighbours (*biased clustering*).

3.5. Simulation of etch rates

In order to determine the etch rate of any crystallographic plane $(h\,k\,l)$, our simulation program creates a Si crystal with the desired $(h\,k\,l)$ orientation and proceeds with the removal of surface atoms according to the microscopic model presented in Sections 3.1 and 3.2, materialised by the use of the removal probabilities presented in Section 3.3. Eventually, as the process carries on, layers of the crystal are completely removed. The etch rate is determined as the ratio of the distance advanced by the surface (i.e. the average height of the surface atoms) to the time evolved (measured as the number of complete surface updates).

The incorporation of partial surface coverage by OH/H into the simulations is done simply by recognising that, if θ is the *nominal value* of the surface coverage by OH (i.e. the fraction of OH-terminated bonds in the surface), the probability with which any dangling bond is terminated by an OH is given by θ. Correspondingly, the probability that a dangling bond is terminated by hydrogen is given by $1 - \theta$, reflecting the fact that, if a dangling bond is not terminated by OH, then it is terminated by H. We note that the incorporation of the coverage dependence in this manner introduces a stochastic component into the Cellular Automaton. However, according to our experience, the parallel updating rule preserves a high level of correlation between the surface sites, still enabling the formation of typical macroscopic features even for the case of systems in the micron scale.

A description of the computational methodology and considerations involved in the determination of the etch rates is given in Appendix A.

4. Results

4.1. Dependence on OH coverage

We determine the effects of simultaneous surface coverage by OH and H on the etching process by analysing two related problems: (i) the dependence of the etch rates on the amount of OH coverage (θ) and (ii) the surface morphology around convex corners for different values of θ. In both cases we use *first termination acceleration* (Appendix A.1) in order to speed up the simulations at low coverage values and *biased maximal clustering* (Section 3.4), because it provides the best match between our simulations for the surface morphology around convex corners and the experiments (see Section 4.1.2). Initial thermalisation is used in (i) but not in (ii), because in this case the presence of the mask enforces the apparition of all possible surface states (Appendix A.2).

The effect of having different OH/OH interaction energies e_{OH}^{TA} is considered. For each value of e_{OH}^{TA}, a value for e_{OH}^{FN} is obtained from Eq. (7). The energies e_{H}^{TA} and e_{H}^{FN} are kept fixed at 0.2 and 0.0 eV, respectively. For the use of Eq. (5), $E_c^A = 2.12$ eV and $T = 348$ K.

4.1.1. Etch rates versus OH coverage

In Fig. 3 we show the etch rates of a representative set of orientations as a function of OH coverage θ for different interaction energies e_{OH}^{TA}. The anticipated dependence of the etch rate on the OH coverage,

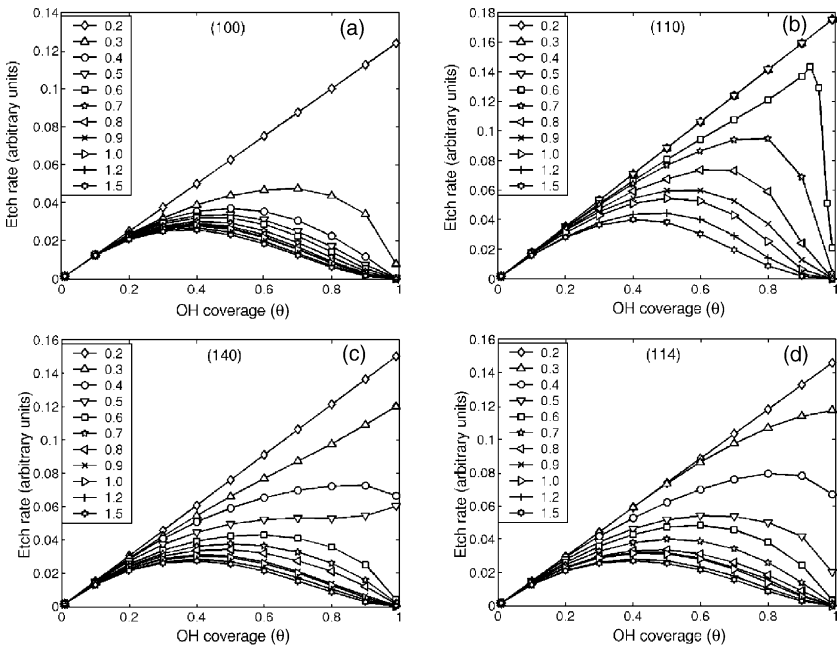

Fig. 3. Dependence of the etch rates of (a) (1 0 0), (b) (1 1 0), (c) (1 4 0) and (d) (1 1 4) on the amount of surface coverage by OH (θ) for different interaction energies $e_{\mathrm{OH}}^{\mathrm{TA}} = 0.2, 0.3, \ldots, 1.5$ eV.

namely, the existence of a maximum (Section 1.1), is confirmed by these results. The figure shows that the position of the maximum is related to the energy of the OH/OH interactions. If the interaction is weak, a linear dependence is observed and no maxima are found. As the interaction is increased, deviations from this linear behaviour occur at the high OH coverage region and the maximum develops. As the interaction energy is increased further, the maximum moves to lower OH coverages and the absolute value of the maximum decreases. This decrease can be attributed to the stiffness presented by the linear behaviour at the low coverage region. The behaviour for other orientations is similar as shown in Fig. 4.

The planar size of the simulated ($h\,k\,l$)-oriented crystals used for the determination of the etch rates is 27 nm × 27 nm. Systems with larger sides (twice, four times and eight times larger) have been checked and no significant differences were found in the converged values of the etch rates.

Experimentally, it is easier to plot the etch rates against the pH (related to the concentration of OH in dissolution) or, more often, against the concentration of the etchant (e.g. [KOH]). It is therefore useful to consider what would be the result of plotting the etch rates of Figs. 3 and 4 against the concentration and not the coverage. Fig. 5 shows the expected qualitative dependence of the surface coverage θ as a function of the concentration of OH ions in solution. Note that the amount of OH coverage saturates for sufficiently large concentrations, since the reaction kinetics at the surface is overwhelmed by the amount of OH ions available. On the other hand, for low enough concentrations, the coverage should increase linearly, because the average distance between OH ions (or OH clusters, if these are formed) attached at the surface is large enough, making it possible for new attachments to occur in between existing ones without any extra interaction. In the intermediate region, no local maxima should be expected, because it would imply the existence of a parabolic minimum in the dissolution of the reaction products as a function of concentration, whilst only a parabolic maximum can be expected in this case. Therefore, the linear behaviour changes monotonically to saturation. Thus, a plot of the etch rates as a function of the concentration of OH in solution will keep the same qualitative shape of Fig. 3 in the linear region and in the region of the

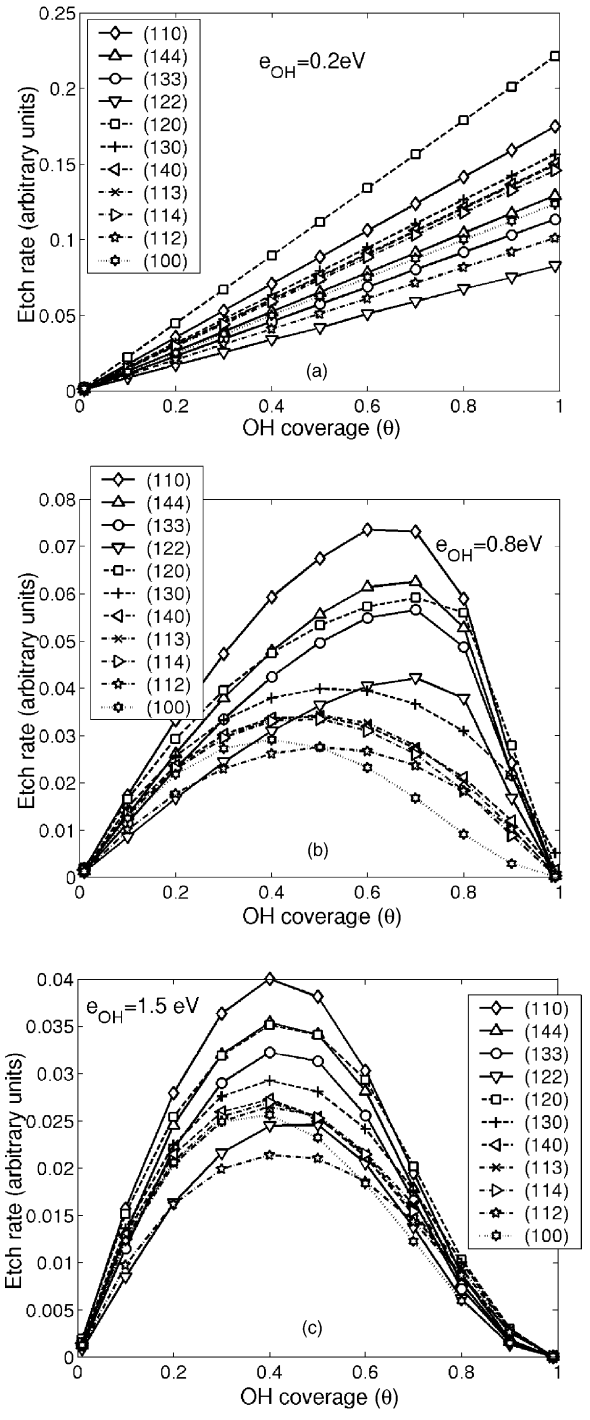

Fig. 4. Etch rates of different orientations ($h\,k\,l$) as a function of OH coverage (θ) for different interaction energies $e_{OH} \equiv e_{OH}^{TA} =$ 0.2 eV (a), 0.8 eV (b) and 1.5 eV (c).

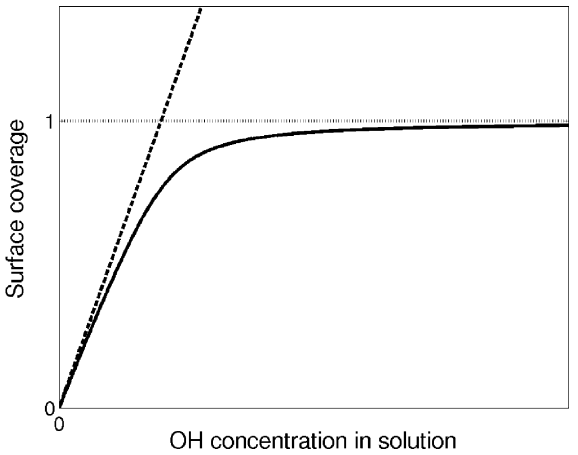

Fig. 5. Qualitative dependence of the surface coverage θ with respect to the concentration of OH ions.

maxima and will only result in a softening of the decay to the right of the maxima.

The existence of maxima in the etch rates as a function of etchant concentration and pH is reported in experiments [18–22]. In some cases, no maxima are observed. We explain this as due to the use of a too restricted range of concentrations in the particular experiments.

We note that the crossing between the etch rates of the different ($h\,k\,l$) orientations observed in Fig. 4 has a direct influence on the under-etching structures observed macroscopically in the presence of masks. The dependence of the fastest-etched orientation compatible with the constrictions imposed by the mask at a certain coverage is contained in these plots (Section 4.1.2).

As pointed out in Section 3.2, a physically meaningful behaviour of the etch rate of any crystallographic plane as a function of the surface coverage conditions requires not only the incorporation of the effects from the ISN_{TA} but also from the ISN_{FN}. Fig. 6 shows the etch rates of different orientations ($h\,k\,l$) as a function of OH coverage θ when the geometrical restrictions imposed by the ISN_{FN} are taken into account (a) and when they are not considered (b). If the geometrical restrictions from only the ISN_{TA} are incorporated (b), only the plane (1 0 0) shows a global maximum. However, when also the geometrical restrictions from the ISN_{FN} are taken into account (a), the maximum develops for all the orientations.

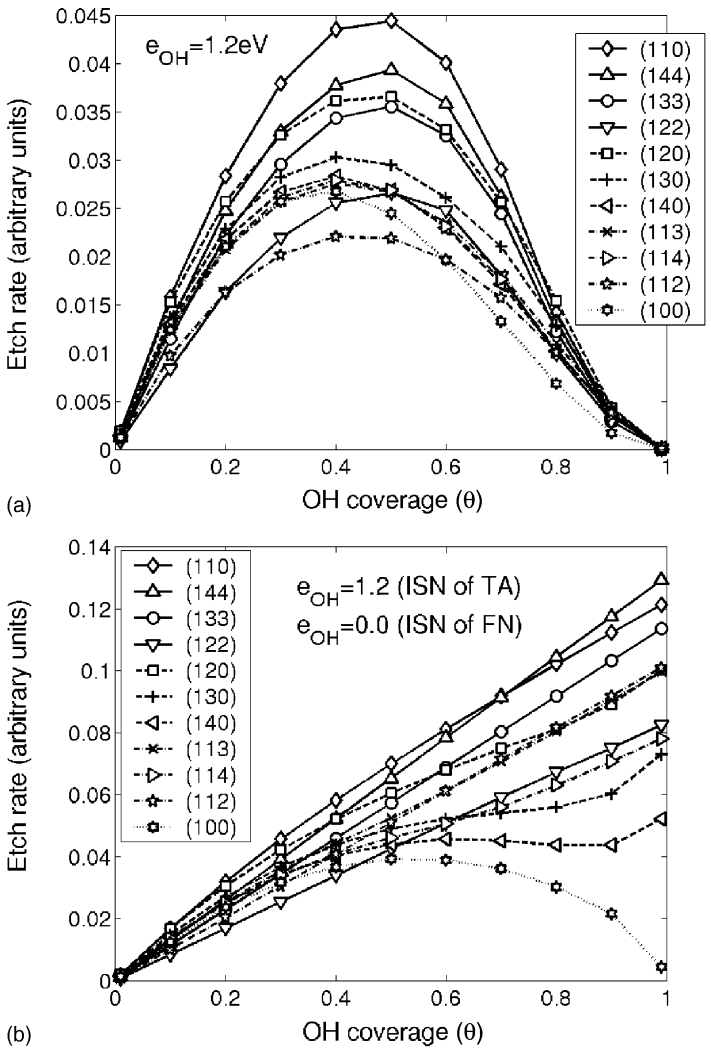

Fig. 6. Etch rates of a representative set of orientations ($h\,k\,l$) as a function of OH coverage θ for (a) $e_{OH} \equiv e_{OH}^{TA} = 1.2$ eV ($e_{OH}^{FN} = 1.0$ eV from Eq. (7)) and (b) when no OH/OH interaction is considered for the ISN_{FN} ($e_{OH}^{FN} = 0.0$ eV).

4.1.2. Convex corner under-etching

We now look at the effects of partial OH coverage on the surface morphology. For that purpose, we consider the underetched structures that appear at the convex corners of square-shaped masks oriented at an angle α with the $\langle 1\,1\,0\rangle$ direction on a Si(0 0 1)-oriented crystal. Fig. 7 shows the structures observed when $\alpha = 0°$ (columns (a) and (b)) and $\alpha = 45°$ (column (c)) for the case of three different coverage values $\theta = 0.01$ (row 1), $\theta = 0.2$ (row 2) and $\theta = 0.7$ (row 3). The planar size of the systems is 0.23 μm × 0.23 μm and the snapshots are taken at the moment when the etched depth is 18 nm. The OH/OH interaction at ISN_{TA} was fixed at 0.6 eV.

As seen from columns (a) and (b), the shape of the underetched structure depends strongly on the amount of OH coverage of the surface. In fact, the dependence is not trivial and it is not always possible to find the crystallographic orientation of all the appearing surface facets. As an example, the orientation of the two lower surface facets in the inset of frame (c.1) cannot be properly determined, although all the surfaces

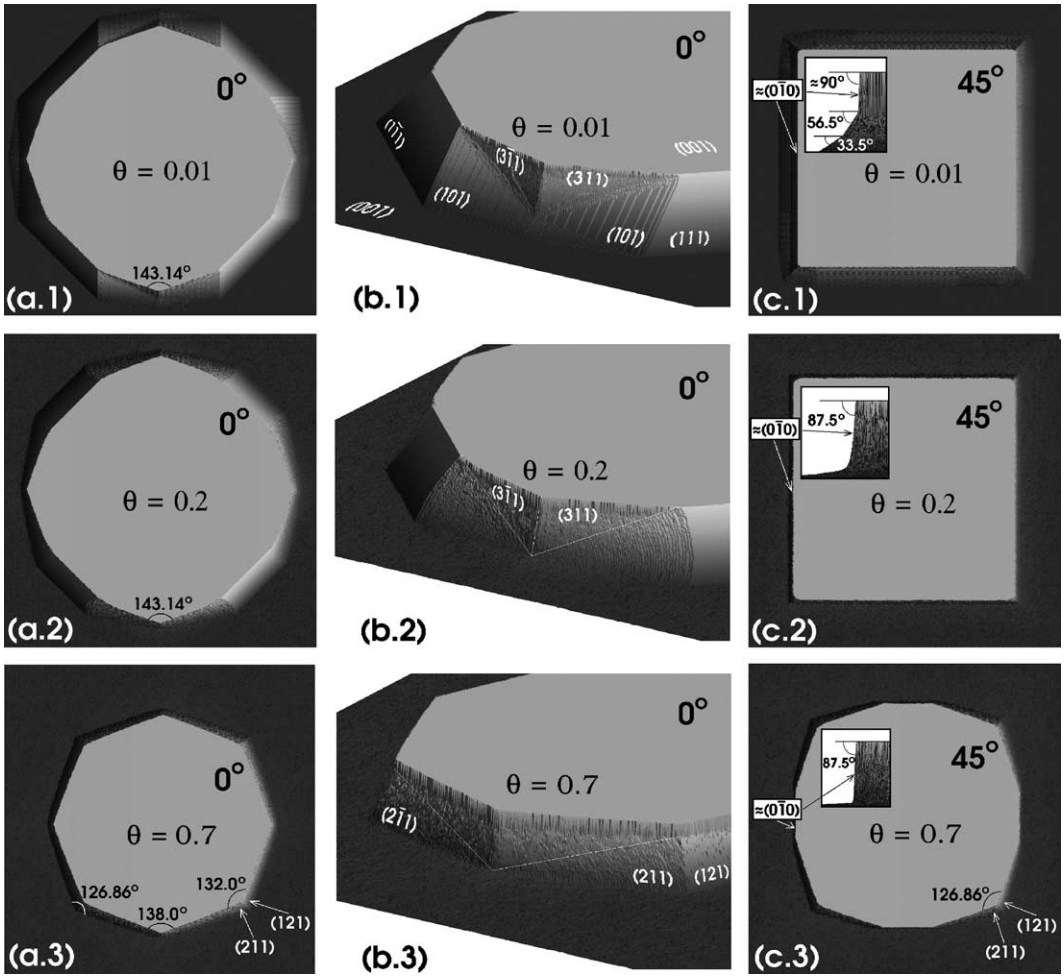

Fig. 7. Surface morphology and under-etching at convex corners of square-shaped masks oriented making an angle $\alpha = 0°$ (columns (a) and (b)) and $\alpha = 45°$ (column (c)) with the $\langle 1\,1\,0\rangle$ direction on a Si(0 0 1)-oriented crystal. Results for three different coverage values $\theta = 0.01$ (row 1), $\theta = 0.2$ (row 2) and $\theta = 0.7$ (row 3) are shown. Each snapshot in column (b) is a close-up detail of the lower corner of each of the snapshots in column (a). The inserts in column (c) show the underetched profiles along the sides. The planar size of the systems is 0.23 μm $\times$0.23 μm. The etched depth is 18 nm in all cases.

appearing in frame (b.1) can be successfully indexed. In the particular case of (c.1), it is still possible to describe the non-crystallographic surface facets as accumulated bunches of (1 1 0) terraces. However, this kind of description is not possible in the case of the 'curved facets' in (b.2), corresponding to (1 0 1) in (b.1); or in the case of the lower region of the inset in (c.2). Another example is that of (3 1 1), which cannot be identified in (b.3) although it is found in (b.1) and (b.2).

The appearance of non-crystallographic surfaces in the simulations is in agreement with the experiments. It can be considered as a signature of the microscopic statistical nature of the etching process, in contrast with traditional Wulff–Jaccodine geometrical approaches [23,24] in which wet chemical etching is considered explicitly at the outset as a macroscopic orientation-dependent process, where *orientation* is understood as *crystallographic orientation*.

The dramatic effects of variations in coverage/concentration on the shape of the underetched structures (as exemplified by column (c)) can be explained as the result of the dependence of the orientation of the

fastest-etched planes on coverage. At low coverage the etch rate of high-index planes such as (2 1 1) is not large enough so as to compete with the (1 0 0) planes (frames (c.1) and (c.2)). However, at higher coverage the (2 1 1) planes become faster than the (1 0 0) planes and, as a result, the (2 1 1) planes appear as the conforming facets at the convex corners (frame (c.3)). In spite of the ability demonstrated by this crystallographic approach to describe the nature of facetting for the particular example of column (c), it should be noted that, in general, considering the etching process simply as the determination of the fastest-etched crystallographic orientation will only provide an incomplete description of the underetched surfaces, as the approach will not be able to predict the appearance of non-crystallographic surface facets. However, with the use of our microscopic model curved under-etching structures are developed in a natural way in the simulations. Besides, the microscopic origin of the change in the orientation of the fastest-etched planes can be identified, as done, e.g. for the case of (1 0 0) and (2 1 1) in Section 5.2.

The microscopic model also reproduces the time evolution of the surface morphology. As an example, the typical time evolution of the undercutting process occurring at the convex corners in Fig. 7(c.3) is presented at the right-hand side column of Fig. 8. In addition, the time evolution for a typical convex corner compensating structure [25] is shown on the left-hand side column of the figure. As in the experiments, the compensating structure provides the elimination of undercutting. The microscopic model

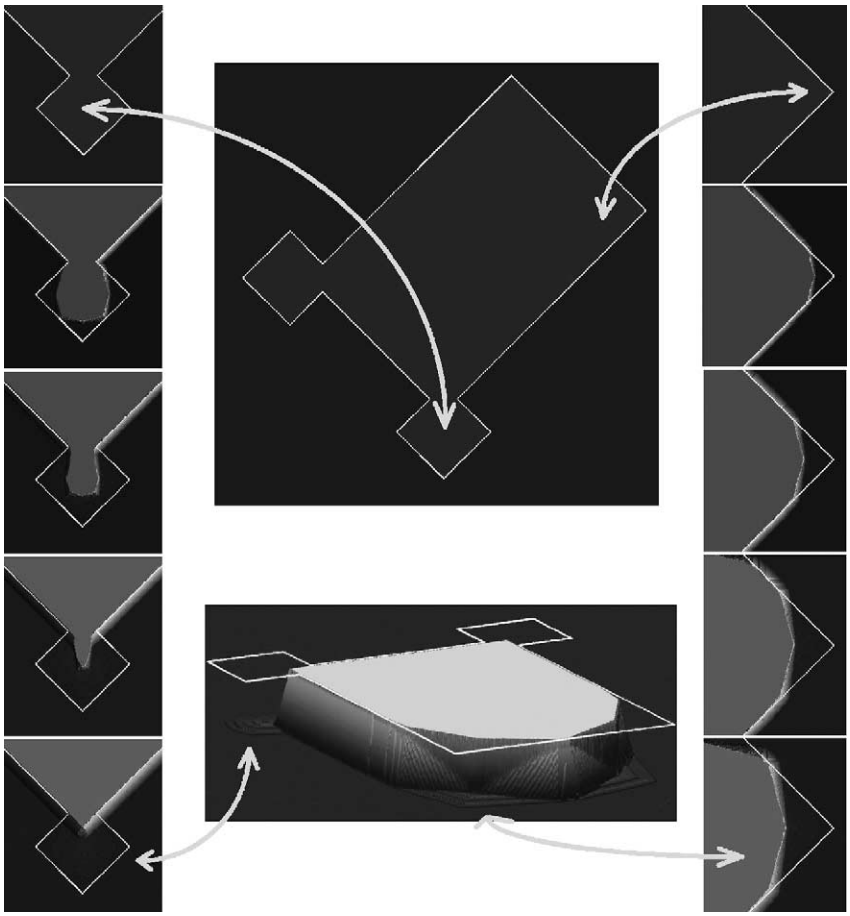

Fig. 8. Time evolution of the etching process around convex corners ($\theta = 0.7$, cf. Fig. 7(a.1)). The planar size of the systems in the central column is 0.23 μm × 0.23 μm.

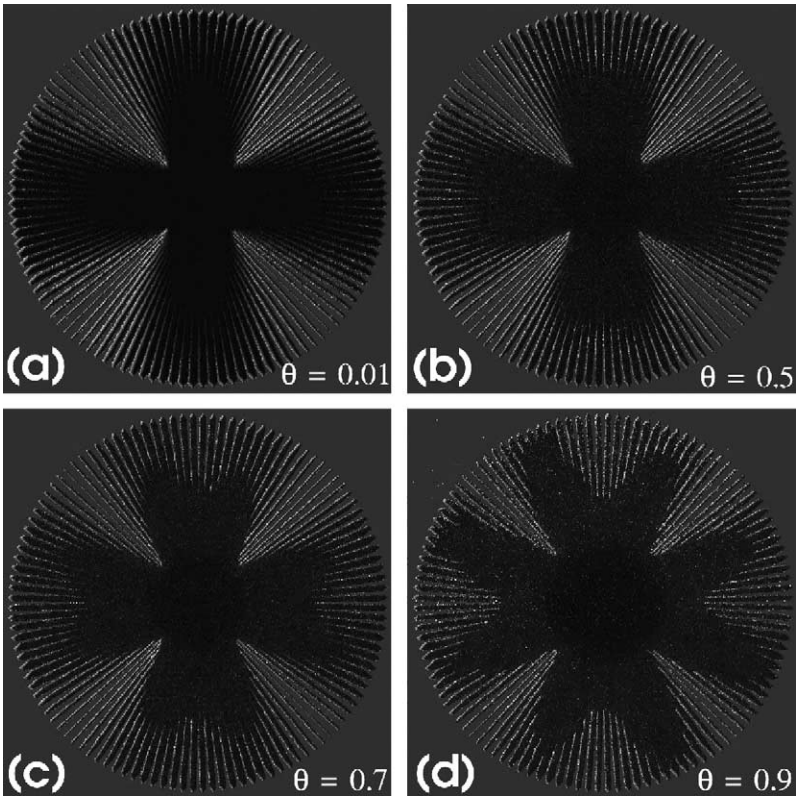

Fig. 9. Etching of Si(0 0 1) wafers masked with a wagon-wheel pattern for different OH coverage values: (a) $\theta = 0.01$, (b) $\theta = 0.5$, (c) $\theta = 0.7$, and (d) $\theta = 0.9$. The planar size of the systems is 0.35 μm × 0.35 μm.

predicts that after a certain time/depth, the corner will present a desired 90° form (as seen from the top).

The dependence of the fastest-etched plane on the amount of OH coverage is best observed with the use of a wagon-wheel masking pattern [26]. Fig. 9 presents the results of simulations of the etching of Si(0 0 1) wafers masked using that pattern, for different coverage values $\theta = 0.01$, $\theta = 0.5$, $\theta = 0.7$, and $\theta = 0.9$. The same interaction energies and methodologies as in the case of the square masks are used. The figure shows that the larger the coverage, the stronger the anisotropy of the pattern. This is due to the fact that, as the amount of OH coverage increases, the etch rate of (1 0 0) planes decreases while the etch rates of other planes might be still increasing. This allows other high-index planes to become the fastest-etched planes, as will be explained in Section 5.

We note that the features of the etching patterns in Figs. 7–9 are the same for systems with larger size. For smaller systems, the fact that below a size of approximately 0.10 μm the simulated patterns depart from the ones seen in the experiments ensures that the features developed in Figs. 7–9 are macroscopic and not microscopic or mesoscopic.

4.2. Dependence on OH clustering

In order to determine the effects that clustering has on the etching process, we modify the probability of OH termination of the dangling bonds of the target atom and of the first neighbours independently and observe the dependence on the coverage θ. For simplicity, we consider two possible situations: (i) no clustering and (ii) biased maximal clustering (see Section 3.4). When clustering is dismissed, the probability with which the dangling bonds of the visited atom and of any neighbour (be it first or second, or further away at any distance) are terminated by OH

groups is given by the nominal value θ of the surface coverage. In the event that the dangling bond is not terminated by OH, then it is terminated by H. In the case of maximal clustering, the dangling bonds of both the visited atom and its first neighbours have unit probability of being OH-terminated, but the second and further neighbours are terminated by OH or H according to θ. In both (i) and (ii), first termination acceleration (Appendix A.1) and initial thermalisation (Appendix A.2) are used.

For the non-clustering case, Fig. 10 shows the etch rates as a function of the nominal coverage θ for a representative set of orientations and for different interaction energies ($e_{OH} \equiv e_{OH}^{TA}$) of 0.2 eV in (a), 0.8 eV in (b) and 1.8 eV in (c). Similarly, for the biased maximal clustering case, Fig. 4 shows the etch rates for the same set of orientations and for the same interaction energies in (a) and (b), and for a similar value of 1.5 eV in (c). In both Figs. 4 and 10, as the interaction energy becomes larger from (a) to (c), the maxima of the etch rates is shifted to lower values of θ. However, in Fig. 10 the etch rates in the low θ region increase according to a power law $R \propto \theta^p$ with $p > 1$ ($p \approx 3.12$ according to Fig. 11), whilst this occurs linearly ($p = 1$) in Fig. 4. The difference is most evident by comparison of Figs. 4(a) and 10(a). From these results we conclude that the existence of clustering is correlated with the behaviour of the etch rate of any crystallographic plane at low OH coverages. Therefore, the existence of clustering can be assessed macroscopically by the determination of the exponent of the power law at low concentrations of the etchant.

5. Pitting and step propagation

As shown in Appendix B.2, the etching process is controlled by only a few surface configurations involving two and three first neighbours and a number of second neighbours ranging from seven to nine. It will be shown in this section that the relative occurrence of etch pitting and step propagation in wet chemical etching is controlled by the removal probabilities of these configurations. As a result, etch pitting and step propagation can be understood as particular realisations of the two microscopic processes considered in this work, namely, backbond weakening and

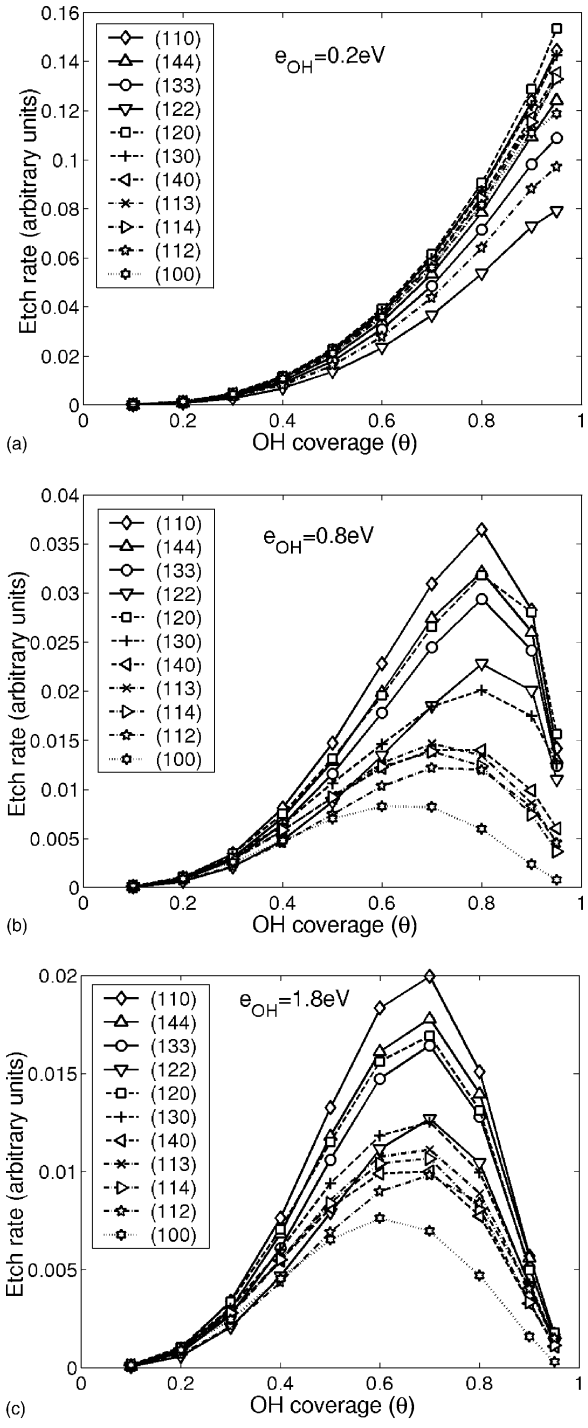

Fig. 10. Etch rates for different surface orientations when clustering is not considered. Compare with Fig. 4 where biased maximal clustering is used.

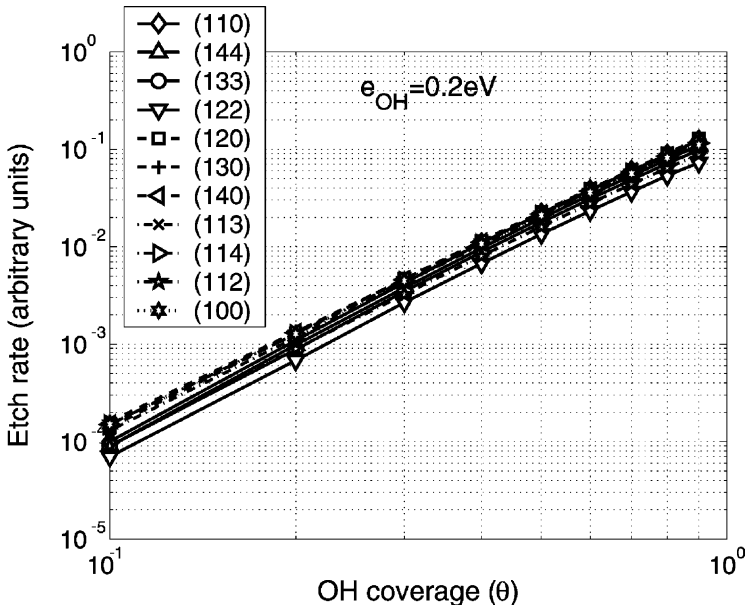

Fig. 11. The log–log plot of the etch rates in Fig. 10(a). The exponents found are: 3.2383 (1 1 0), 3.2309 (1 4 4), 3.1969 (1 3 3), 3.1765 (1 2 2), 3.1036 (1 2 0), 3.0294 (1 3 0), 3.0370 (1 4 0), 3.0908 (1 1 3), 3.0367 (1 1 4), 3.1372 (1 1 2) and 3.0185 (1 0 0).

the existence of interactions between the terminating species in the presence of indirect second neighbours.

Although wet chemical etching is a complicated process involving a large amount of surface reactions and configurations, the fact that the essential features of the process are controlled by only a few surface configurations allows a certain level of simplification in the analysis of the surface morphology and its relevant features. Only the *average* surface morphology needs to be considered whilst the statistical fluctuations may be disregarded. Since the etching process is biased towards the removal of layers in the Cellular Automaton approach, the average morphology is then closely related to the morphology of the ideal surfaces.

5.1. Key surface configurations

We proceed first with the identification and description of the key surface configurations at the different surface orientations.

5.1.1. Key configurations at Si(1 1 1)

Consider the ideal (1 1 1) surface depicted in Fig. 12. An example of a typical atom of this surface is atom A in Fig. 12(a), having three first neighbours and nine second neighbours. If we use the notation (n_1,n_2) to refer to any atom with n_1 first neighbours and n_2 second neighbours, atom A is identified as (3,9). Since the removal of this type of atom will initiate an etch pit, the corresponding removal probability $p(3,9)$ can be associated to the rate of pit generation at (1 1 1) planes. Similarly, the rate of propagation of $[1\,\bar{2}\,1]$ steps at (1 1 1) surfaces (such as step *pq* in Fig. 12(b); cf. Fig. 13(a)) is determined by the removal probability $p(3,7)$ of atoms such as A in Fig. 12(b) with three first neighbours and seven second neighbours. Note that the other type of atom in the step (e.g. B in Fig. 12(b)) is completely equivalent to A and, therefore, the removal probability $p(3,7)$ fully controls the propagation of $[1\,\bar{2}\,1]$ steps. In a similar way, the removal probability $p(2,7)$ of atoms such as A in Fig. 12(c) controls the rate of $[\bar{1}\,2\,\bar{1}]$ step propagation (e.g. step *rs* in Fig. 12(c)). Note that the time evolution of this step will bring to the surface atoms such as B, also characterised by $p(2,7)$. The etching process at (1 1 1) surfaces is thus controlled by $p(3,9)$ through the generation of etch pits and, by $p(3,7)$ and $p(2,7)$ through the propagation of $[1\,\bar{2}\,1]$ and $[\bar{1}\,2\,\bar{1}]$ steps, respectively.

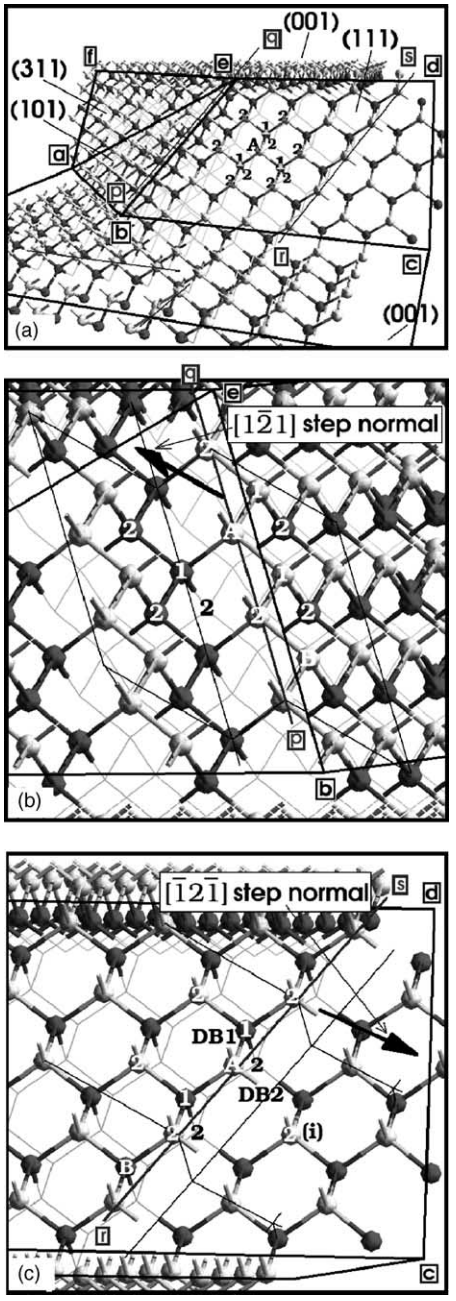

Fig. 12. (a) An underetched convex corner at low θ (cf. Fig. 7(b.1)). Only one-half of the symmetrical structure is shown. Closer views of (b) $[1\ \bar{2}\ 1]$ step and (c) $[\bar{1}\ 2\ \bar{1}]$ step are shown from arbitrary directions. Surface atoms are shaded lighter and backbonded atoms darker. Steps are characterised by the direction of their normal. First and second neighbours are labelled as **1** and **2**, respectively. Indirect second neighbours are additionally marked with (**i**). Boxed letters are used to ease comparison between (a), (b) and (c).

5.1.2. Relation to microscopic processes

It is worth considering the nature of the microscopic processes determining the values of $p(3,9)$, $p(3,7)$ and $p(2,7)$. As Fig. 12(a) and (b) show, both (3,9) and (3,7) atoms have no indirect second neighbours. Thus, the values of the corresponding removal probabilities $p(3,9)$ and $p(3,7)$ are determined by the bond-weakening mechanism only. Since two of the first neighbours of atom A in Fig. 12(b) are also in the etch front, OH groups can be attached to them and result into further weakening of the backbonds of atom A. In this way, the energy of two of the backbonds is decreased further with respect to the case of atom A in Fig. 12(a). This makes the removal of (3,7) easier than that of (3,9). Thus, $p(3,9)$ is typically small compared to $p(3,7)$ and the etching of (1 1 1) surfaces occurs as a 'peeling off' process [27], resulting from the propagation of steps driven by the larger values of $p(3,7)$ (and $p(2,7)$ at low coverages).

In the case of atom A in Fig. 12(c), the appearance of one indirect second neighbour (i) reduces the probability of OH termination of the dangling bond DB2 with respect to that of DB1. Note that the probability of OH termination in the presence of indirect second neighbours depends strongly on coverage/concentration. At low coverage, OH/OH interactions occur rarely since the probability of finding an OH attached to the indirect second neighbour simultaneously to the attachment of an OH to DB2 is very low. Thus, OH termination of the two dangling bonds DB1 and DB2 occurs rapidly once any of them has been OH terminated, due to the driving effect of OH clustering. However, at higher coverages, the interaction between the terminating OHs (at DB2 and the indirect second neighbour) occurs more frequently and, as a result, the probability of OH termination of DB2 is reduced. Correspondingly, the probability of removal of atom A is also reduced, thus leading to a reduction in the rate of step propagation. In addition, after the removal of atoms such as A, it will be the turn for the removal of atoms such as B, having two indirect second neighbours. The presence of one more indirect neighbour reduces the removal probability even further for moderate and higher coverages and therefore the removal of these atoms can become a bottle-neck for the propagation of $[\bar{1}\ 2\ \bar{1}]$ steps. As we see, depending on coverage/concentration, the ratio between the rates of propagation of $[\bar{1}\ 2\ \bar{1}]$ and $[1\ \bar{2}\ 1]$

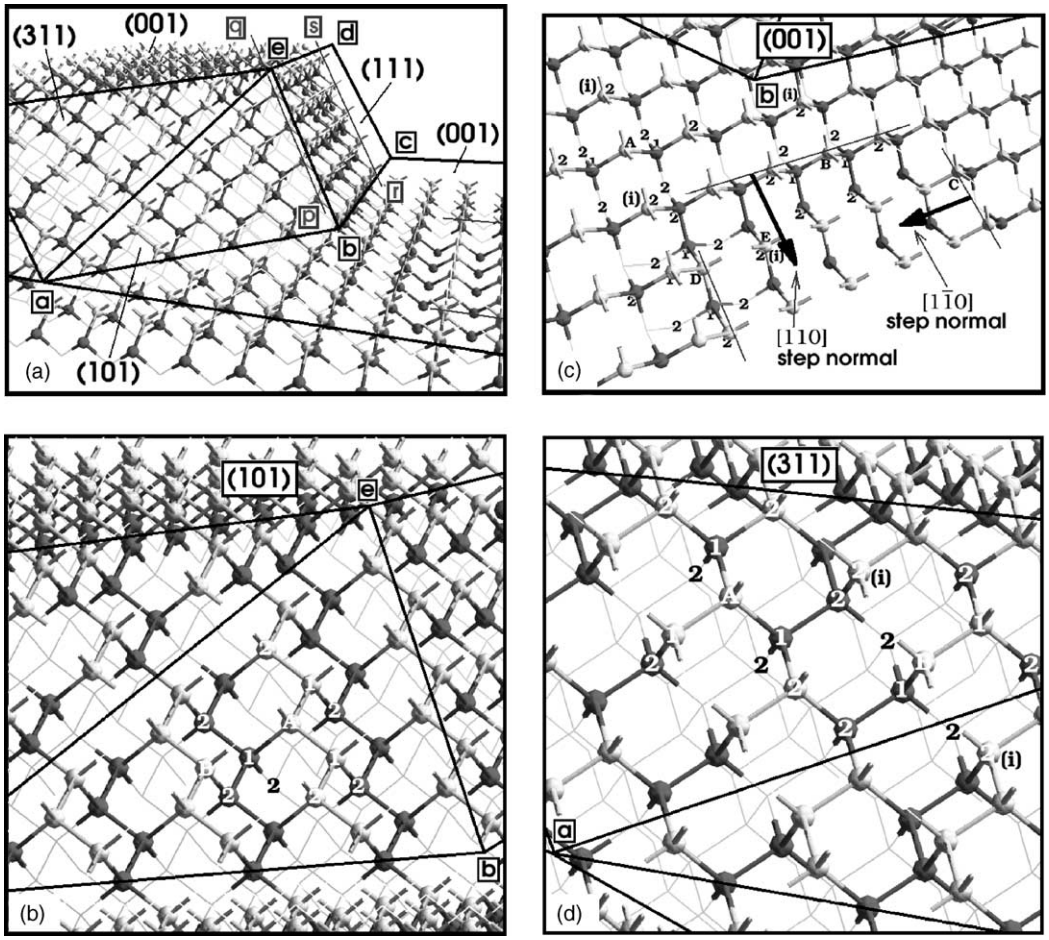

Fig. 13. (a) An underetched convex corner at low θ (cf. Fig. 7(b.1)). Only one-half of the symmetrical structure is shown. Closer views of (b) (101) plane, (c) (0 0 1) plane with several $\langle 1\,1\,0\rangle$ steps, and (d) (3 1 1) plane are shown from arbitrary directions. Labelling and shading as in Fig. 12.

steps can be larger or smaller. For higher coverages the bottle-neck at $[\bar{1}\,2\,\bar{1}]$ steps will be so pronounced that the etching of (111) will proceed essentially by only $[1\,\bar{2}\,1]$ step propagation.

5.1.3. Key configurations at other orientations

Let us now consider the situation at other surface orientations. Since any surface atom at an ideal (1 1 0) plane (such as atoms A and B in Fig. 13(b)), has three first neighbours and seven second neighbours, the removal probability $p(3,7)$ also controls the etch rate of (1 1 0) surfaces. Similarly, a typical atom at an ideal (1 0 0) surface (atom A in Fig. 13(c)) has two first neighbours and eight second neighbours (cf. Fig. 1(a)) and, therefore, the removal probability $p(2,8)$ determines the rate of pit generation at ideal (1 0 0) surfaces. In turn, the removal probability $p(2,7)$ of atoms like B and C in Fig. 13(c) determines the rate of propagation of [1 1 0] and $[1\,\bar{1}\,0]$ steps at (1 0 0) surfaces. Note that, for $[1\,\bar{1}\,0]$ and $[\bar{1}\,1\,0]$ steps, also atoms like D are present, but these have three first neighbours and eight second neighbours (one of them indirect) and, therefore, lower removal probabilities $p(3,8)$ than $p(2,7)$ (one indirect neighbour also but only two first neighbours).

The rate of pit generation at a typical high-index plane such as (3 1 1) is controlled by $p(3,7)$ and $p(2,7)$ (atoms A and B in Fig. 13(d)). Note that for both

(1 1 0) and (3 1 1) there is no need to consider step propagation (as is necessary for (1 1 1) and (1 0 0)), because the probabilities $p(3,7)$ and $p(2,7)$ are typically large enough (in opposition to $p(3,9)$ and $p(2,8)$), making etch pitting the dominant mechanism at these orientations. Since the determination of the removal probability $p(2,7)$ involves one indirect second neighbour, the etch rate of (3 1 1) is more strongly dependent on coverage than the etch rate of (1 1 0), which is purely determined by bond-weakening.

5.1.4. Different mechanisms for etch pitting

It is important to notice that the etch pitting mechanism at (1 0 0) surfaces is controlled by a different microscopic mechanism than at (1 1 1). In (1 0 0) the removal probability $p(2,8)$ is to a large extent determined by the existence of two indirect second neighbours (atom A in Fig. 1(a) and in Fig. 13(c)) and, as a result, it is strongly dependent on coverage/concentration, as in the case of (2,7) discussed above. However, pitting at (1 1 1) is controlled by bond-weakening and, therefore, the dependence on coverage is smoother. This agrees well with the fact that Si(1 1 1) surfaces are typically smooth as compared to Si(0 0 1) surfaces.

5.2. Fastest-etched plane orientation

The previous considerations explain why the orientation of the fastest-etched plane is strongly sensitive to the amount of coverage by OH. Through the geometrical restrictions from the indirect second neighbours, the amount of OH coverage θ fixes the relative value of the removal probabilities $p(2,7)$ and $p(2,8)$ with respect to $p(3,7)$ and $p(3,9)$, i.e. the relative occurrence of step propagation and pitting at all orientations. Thus, for coverage values providing large $p(2,7)$ and $p(2,8)$ as compared to $p(3,7)$, the (1 0 0) surfaces will become the fastest-etched planes. However, if both $p(2,7)$ and $p(2,8)$ are moderate and $p(3,7)$ is large enough, (1 1 0) will be the fastest-etched plane, and if $p(2,7)$ and $p(3,7)$ are large enough and $p(2,8)$ is moderate, a high-index plane (e.g. (3 1 1)) will be the fastest-etched plane. The dependence of the orientation of the fastest-etched planes on coverage can be seen as a signature of the geometrical restrictions imposed by the indirect second neighbours.

As an example, we may consider why the etch rate of (2 1 1) is lower than that of (1 0 0) at low coverages but larger at higher coverages (column (c) of Fig. 7). For the case of (2 1 1) planes, the etch rate is controlled by $p(2,7)$ and $p(3,9)$, as these surfaces can be considered as bunched (1 1 1) terraces with $[\bar{1}\,2\,\bar{1}]$ steps. The appearance of (1 1 1) terrace atoms (just like A in Fig. 12(a)) at this orientation implies that the etch rate is controlled by the propagation of $[\bar{1}\,2\,\bar{1}]$ steps. At low coverage, the combined effect of $p(2,7)$ and $p(3,9)$ in (2 1 1) cannot compete with the etch rate given by $p(2,8)$ in (1 0 0). However, as the coverage increases, $p(2,8)$ decreases more than $p(2,7)$, because it involves two indirect second neighbours instead of one, thus making the interactions between the terminating OHs have a stronger effect on the etch rate of (1 0 0). Therefore, the etch rate for (1 0 0) becomes lower than that of (2 1 1). This has dramatic effects on the shape of the under-etching features, as shown in column (c) of Fig. 7.

6. Discussion

According to Allongue [4], the rate-limiting step for the formation of a Si complex solvable in the solution is the first substitution of a terminating H by an OH, after which the sequence of further chemical steps is fast. The mechanism of this first substitution is the only difference between the chemical and the electrochemical routes [3]. The chemical route, which has a low activation barrier, represents an anisotropic contribution to the etching process, because it can only occur at kink sites. On the other hand, the electrochemical route, which implies a high activation barrier, represents an isotropic contribution, because it occurs at all surface sites. However, the fact that the first H substitution by OH is significantly restricted at certain configurations involving next-nearest neighbours (as we have stressed in this work) means that the isotropic contribution to the etching process (the electrochemical reaction) is actually *not so isotropic*. Probably the reason why this feature has not been realised before is that, in fact, the anisotropy of the etching process is partly explained by peeling off and etch pitting of (1 1 1) surfaces, i.e. the microscopic mechanisms accessed by the electrochemical studies of the (1 1 1) surfaces. However, the rest of the

anisotropy, especially the appearance of high-index fastest-etched planes, cannot be probed by this approach because it is not controlled by these mechanisms, but by the geometrical restrictions imposed by the indirect second neighbours, most visible in the etching of (1 0 0) surfaces and other high-index fastest-etched surfaces.

Schröder and Obermeier [27] have presented a 'step flow model of 3D structuring' for anisotropic etching in $Si_{\{1\,0\,0\}}$ using only the etch rate in the direction $[1\,\bar{2}\,1]$ $R_{[1\,\bar{2}\,1]}$ (i.e. the rate of propagation of $[\bar{1}\,2\,\bar{1}]$ steps[2]), and the etch rate of (0 0 1) planes $R_{(0\,0\,1)}$. Since only the number of broken bonds to the first neighbours is considered but no attention is paid to the effects from second neighbours, they conclude erroneously that $R_{[1\,\bar{2}\,1]}$ is always higher than $R_{[\bar{1}\,2\,\bar{1}]}$ (two and three first neighbours, respectively). As explained in Section 5.1.2, $R_{[1\,\bar{2}\,1]}$ becomes much smaller than $R_{[\bar{1}\,2\,\bar{1}]}$ at high coverages.

Our microscopic model provides an answer to the question raised in [27] about the relation between $R_{[1\,\bar{2}\,1]}$ and $R_{(0\,0\,1)}$. The model establishes the connection between the two microscopic processes responsible for wet chemical etching on the atomistic scale (namely, backbond weakening and the geometrical restrictions by the ISNs) and the two mechanisms traditionally considered (namely, etch pitting and step propagation, see Section 5 for details). The physical connection between $R_{[1\,\bar{2}\,1]}$ and $R_{(0\,0\,1)}$ lies in the fact that both rates are controlled by the geometrical restrictions imposed by the indirect second neighbours through $p(2,7)$ and $p(2,8)$.

In addition to $R_{[1\,\bar{2}\,1]}$ and $R_{(0\,0\,1)}$, also the etch rate in the direction $[\bar{1}\,2\,\bar{1}]$ $R_{[\bar{1}\,2\,\bar{1}]}$ and the etch rate of (1 1 1) planes $R_{(1\,1\,1)}$ have a role in the etching process. However, in light of the under-etching results of Section 4.1.2, where non-crystallographic 'curved' bounding surfaces were obtained, we feel the need to stress that *wet chemical etching of crystalline Si should be considered as an atomistic process and not as a macroscopic process involving the etch rates of a few planes and steps*. The latter approach will always provide flat-facetting of under-etching features, only partially in agreement with experiment, while the atomistic approach leads to more realistic features.

[2] Note that a step is defined by its normal and the step propagates in the direction opposite to that normal.

7. Conclusions

We have presented a generalisation of the averaged interaction energetics between surface-terminating hydrogens and hydroxyls [5] with the aim of incorporating explicitly the different interactions into atomistic simulations of anisotropic wet chemical etching of crystalline silicon using a Continuous Cellular Automaton. This has provided a suitable framework for studying the effects of surface coverage and clustering by OH radicals on the etching process.

It has been shown that, for every crystallographic orientation, the etch rate is a non-monotonic function of the amount of OH coverage and, therefore, of the concentration of OH in solution. In particular, we have shown that there always exists a value of coverage for which the etch rate reaches a maximum, in agreement with experiments for scattered orientations [18–22]. The existence of these maxima is directly related to the interactions between the hydroxyls terminating the dangling bonds of the surface atom and its nearest neighbours, and the terminating species (H and/or OH) at next-nearest neighbours.

The dependence of the fastest-etched plane orientation on coverage is implicitly contained in the model and predictions of convex corner under-etching structures are made. The predictive power of the model goes beyond that of traditional geometrical approaches. In addition to the flat (crystallographic) facetting provided for the underetched structures by these methods, non-crystallographic 'curved' bounding surfaces are developed in our simulations, in agreement with experiments. This feature allows for more realistic design and testing of compensating structures to eliminate under-etching effects, as has been shown for a particular geometry.

A prediction has been made for the dependence of the etch rate on concentration at the low concentration region. According to our simulations, the etch rate is described by a power law $R \propto \theta^p$ with $p > 1$ for conditions preventing clustering of OH groups. However, the behaviour is linear if clustering takes place. Thus, the existence of clustering in an experiment can be assessed macroscopically by the determination of the exponent of the power law at low concentrations of the etchant.

Finally, by interpreting the microscopic model used, we have shown that the microscopic mechanism controlling the generation of etch pits at (111) and

(1 0 0) ideal surfaces is different. For the former, the mechanism is backbond weakening and, for the latter, the geometrical restrictions by the indirect second neighbours. As a result, the generation of pits at (1 0 0) depends more critically on the amount of OH coverage than at (1 1 1). We have also shown that the dependence of the orientation of the fastest-etched plane on coverage is controlled by only a few surface configurations involving indirect second neighbours, and that the relative value of the corresponding removal probabilities determines the relative occurrence of step propagation and etch pitting. As a result, etch pitting and step propagation can be understood as particular realisations of the two microscopic processes considered in our model, namely, backbond weakening and the geometrical restrictions imposed by the indirect second neighbours.

Acknowledgements

This research has been supported by the Academy of Finland through the Centres of Excellence Programme (2000–2005). We would like to thank A. Ayuela for useful discussions.

Appendix A. Simulation of etch rates

In this appendix, we comment on the major considerations involved in the computational determination of the etch rates.

A.1. First termination acceleration

In the case of low θ, the probability that the dangling bonds are OH-terminated is very low and very few backbonds are susceptible for thermal breaking. This leads to a situation where most of the computational time is spent waiting for the occurrence of successful configurations. The problem originates from the fact that, on average, we need to visit an atom $1/\theta$ times before the first OH group is attached to it. This can be overcome by accelerating this first termination and compensating the time measure correspondingly. In other words, every visited atom is assumed to be terminated by one OH and time is modified from t to t/θ. Alternatively, the etch rate has to be multiplied by θ to convert the result to the value that would be obtained without acceleration.

We note that *first termination acceleration* is (statistically) exact for Monte Carlo schemes. However, in the case of a Cellular Automaton, the method introduces additional coupling for the evolution of the surface atoms.

A.2. Thermalisation

Since we use a Continuous Cellular Automaton (in which all equivalent sites evolve exactly identical if they have been exposed to the etchant for exactly the same number of time steps), the simulation of the etching process occurs with a more macroscopic flavour than, e.g. in a Monte Carlo scheme. In other words, the removal of material is more biased towards removal of complete layers than towards removal of individual atoms. In this way, in the case of an ideally flat initial surface, it is possible that some particular surface configurations will be never disclosed, and, as a result, the simulation might represent a situation far from reality. It is thus necessary to provide an initial surface in which as many surface configurations as possible are present, so that the simulated process will guide itself towards a converged stationary state of the surface. Therefore, we prepare the initial surface by a *thermalisation* procedure, eventually leading to a surface with a characteristic composition and roughness far away from the ideally flat surface. In practice, the thermalisation is realised by proceeding with the removal of several layers of atoms without the use of first termination acceleration.

We note that thermalisation is not required for simulations in the presence of masks, since the masks themselves force the apparition of all the possible types of surface sites.

A.3. Convergence

Typically, as the simulated process finds its way towards a converged stationary state of the surface, a first stage can be distinguished in the evolution of the surface, during which the roughness of the surface builds up [9]. This occurs superimposed to the advancement of the surface and, if it takes long, this can increase the number of time steps required to obtain a converged measure of the etch rate. Some-

times, after this stage is over, the etch rate may oscillate around a certain value due to the existence of cycles in the type of configuration which dominates at the surface. This is a signature of the Cellular Automaton scheme, which biases the surface evolution towards the removal of complete layers instead of single atoms. The oscillations are rarely observed when Monte Carlo schemes are used. In such cases, the value around which the etch rates oscillate is taken as the *converged value*. The values of the etch rates presented in this work are always converged values.

Appendix B. Other expressions for the removal probabilities

Similar results to those presented in this work for the wagon-wheel masking pattern are reported in [5,8]. In this appendix, we consider the differences in the expressions for the removal probabilities and the analogies between the three approaches.

B.1. Cohesive versus total energy

In [5], the probability of removal of a surface atom is defined as the probability of breaking the average bond corresponding to the particular configuration shown by the neighbourhood. This is given by the Boltzmann expression:

$$p = \mathrm{e}^{-\Delta E/k_\mathrm{B}T}. \tag{B.1}$$

The energy excess $\overline{\Delta E}$ is defined as:

$$\overline{\Delta E} = k_\mathrm{B}T\,\ln\left[1+\mathrm{e}^{(\bar{E}-E_\mathrm{c})/k_\mathrm{B}T}\right], \tag{B.2}$$

where $\bar{E}$ is the *average energy per bond* and E_c is a critical energy (similar to E_c^A) acting as a threshold below which the probability of breaking one bond is $p \approx 1$. Note that $\overline{\Delta E}$ is approximated by

$$\overline{\Delta E} \approx \max(0, \bar{E} - E_\mathrm{c}), \tag{B.3}$$

the full equality taking place at $T = 0$ K. The average energy per bond $\bar{E}$ is assigned to the chosen surface atom in a similar manner as in the present work. If the chosen target atom has n first neighbours ($n = 1, 2, 3$) and each of them has itself m_j first neighbours ($j = 1, 2, \ldots, n$; $m_j = 1, 2, 3, 4$), l of which are indirect second neighbours to the chosen atom ($l \equiv l_\mathrm{TA}^\mathrm{OH} + l_\mathrm{TA}^\mathrm{H}$), the average energy per bond $\bar{E}$ is defined as

$$\bar{E} = \frac{1}{n}\sum_{j=1}^{n} \epsilon_{(4-n),(4-m_j)} + le(1-\delta_{1n}). \tag{B.4}$$

The first term corresponds simply to the average of the sum of the energies of the bonds to the n first neighbours, the energy of each bond being obtained by looking at the number of hydroxyls attached to both atoms sharing the bond ($i = 4 - n$ and $j = 4 - m_j$). The second term incorporates the effect from indirect neighbours. It contains the *average* energy e for each present indirect second neighbour of the target atom. The variable e is meant to be an average of the H/OH and OH/OH interactions (see Section 3). Note that the indirect second neighbours of the first neighbours are not considered, and that conditions of maximal clustering are assumed and either complete OH termination or complete H termination is assumed for the rest of the dangling bonds, since the interest is only on the average value of the H/OH and OH/OH interactions.

The probability of removal of a surface atom should not be identified with the probability of breaking the average bond, but with the product of the probabilities of breaking each of the n bonds:

$$p = (\mathrm{e}^{-\Delta E/k_\mathrm{B}T})^n = \mathrm{e}^{-n\Delta E/k_\mathrm{B}T}, \tag{B.5}$$

$$\approx \mathrm{e}^{-n\max(0,\bar{E}-E_\mathrm{c})/k_\mathrm{B}T}, \tag{B.6}$$

$$= \mathrm{e}^{-\max(0,n\bar{E}-nE_\mathrm{c})/k_\mathrm{B}T}, \tag{B.7}$$

$$= \mathrm{e}^{-\max(0,E-E_\mathrm{c}^A)/k_\mathrm{B}T}, \tag{B.8}$$

$$\approx \mathrm{e}^{-\Delta E/k_\mathrm{B}T}. \tag{B.9}$$

Here we have used Eq. (B.3) to pass from Eq. (B.5) to Eq. (B.6), we have defined $E_\mathrm{c}^A \equiv nE_\mathrm{c}$ and

$$E \equiv n\bar{E} = \sum_{j=1}^{n} \epsilon_{(4-n),(4-m_j)} + nle\cdot(1-\delta_{1n}), \tag{B.10}$$

in Eq. (B.8). We have also defined ΔE as in Eq. (5) and used that $\Delta E \approx \max(0, E - E_\mathrm{c}^A)$ in Eq. (B.9). Equating the second term of Eq. (B.10) with the second and third terms of Eq. (6) in the main text allows us to find a value of the average energy e in terms of the other parameters. This shows that the two approaches are related in a simple manner and explains why the corresponding results in the simulations are so similar.

In some sense, one can say that the difference between $\bar{E}$ and E is the same difference as between the cohesive energy and the total energy.

Comparison of Fig. 9(c) with Fig. 4(c) in [5] allows identification of the amount of surface coverage by OH to be $\theta \approx 0.7$ in that work. We note, however, that this value of θ depends on the choice of the OH/OH interaction energies ($e_{\mathrm{OH}}^{\mathrm{TA}} = 0.6$ eV and related values from Eqs. (7) and (8)) in such a way that lower θ values will correspond for higher OH/OH interactions.

B.2. Removal probability function

The dependence of the removal of a surface atom on the number of OH groups terminating its first neighbours (backbond weakening) can be understood as a dependence on the number of next-nearest neighbours. This is so because the hydroxyl groups are located at the positions occupied earlier by the next-nearest neighbours of the surface atom. Therefore, different surface atoms having the same number of nearest neighbours but different numbers of next-nearest neighbours will have different removal probabilities. The probability of removal of a surface atom can be written as a function of the number of first and second neighbours (n_1 and n_2, respectively) [8]:

$$p(n_1, n_2) = p_0 \frac{1}{1 + \mathrm{e}^{\beta\epsilon_1(n_1 - n_1^0)}} \frac{1}{1 + \mathrm{e}^{\beta\epsilon_2(n_2 - n_2^0)}}. \quad \text{(B.11)}$$

Here $\beta = 1/k_{\mathrm{B}}T$, $p_0 = (1 + \mathrm{e}^{-\beta\epsilon_1 n_1^0})(1 + \mathrm{e}^{-\beta\epsilon_2 n_2^0})$ is used to satisfy $p(0,0) = 1$ and ϵ_1, ϵ_2, n_1^0 and n_2^0 are parameters of the model described in [8]. A plot of this removal probability function (RPF) is shown in Fig. 14.

By using the microscopic model of the present work, it is possible to explain the remarkable performance [8] of the RPF approach. As compared to the present model, the RPF provides an incomplete, degenerate set of removal probabilities since it associates the same probability of removal to atoms with different numbers of direct/indirect second neighbours, as far as their sum amounts to the same total number of second neighbours. On the contrary, the present model provides access to the complete, non-degenerate set of probabilities. For comparison, it is possible to reduce this non-degenerate set to a degenerate set by simply averaging the removal probabilities of the atoms having the different numbers of direct and

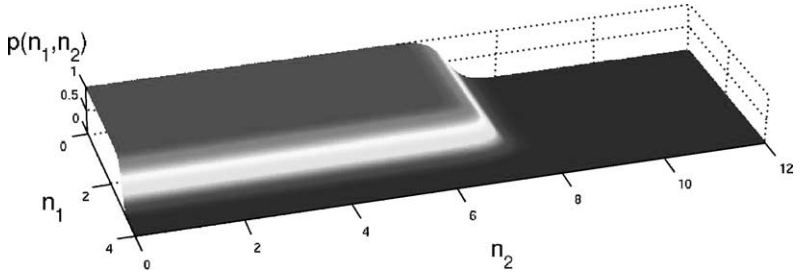

Fig. 14. Removal probability function at $T = 348$ K (75 °C) when the model parameters take the values: $\epsilon_1 = 0.35$ eV, $\epsilon_2 = 0.16$ eV, $n_1^0 = 3.0$ and $n_2^0 = 7.0$.

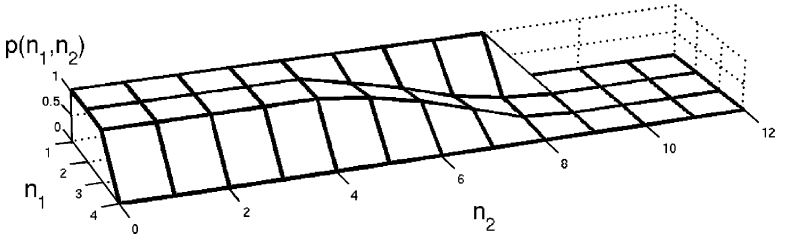

Fig. 15. A typical set of removal probabilities during the simulation of Fig. 9(c).

indirect second neighbours which add up to the same total number. As an example, Fig. 15 shows the plot of one typical average set obtained during the simulation of Fig. 9(c).

By comparison of Figs. 14 and 15 we see that the major trend of the functions is the same. There exist some deviations but, in light of the performance of both models, these are not essential for the understanding of the major macroscopic features of anisotropic wet chemical etching. The two sets of removal probabilities coincide in the existence of significant decrease in the removal probability when the number of second neighbours is increased over a certain value. For instance, for the RPF model, the removal probability has the fastest decrease when the number of second neighbours is increased from 6 to 8 (in the case $n_1 = 2$) and from 7 to 9 (when $n_1 = 3$). By interpreting this result, we conclude that the physical reason why the use of a RPF function produces a good agreement with experiments lies in the fact that it provides a good distinction between the two pairs of surface atoms which, *on average*, have the most relevant roles in the etching process: on the one hand, the pair (2,7)–(2,8), whose removal probabilities control (on average) the etch rate of the (1 0 0) planes (as well as of high-index planes such as (2 1 1) and (3 1 1)) and, on the other hand, the pair (3,7)–(3,9), which controls (on average) the etch rates of (1 1 0) and (111) planes (as well as of high-index planes such as (3 1 1)).

References

[1] W. Lang, Mater. Sci. Eng. R: Rep.: Rev. J. 17 (1) (1996) 1–55.
[2] P. Allongue, V. Costa-Kieling, H. Gerischer, J. Electrochem. Soc. 140 (4) (1993) 1009–1018.
[3] P. Allongue, V. Costa-Kieling, H. Gerischer, J. Electrochem. Soc. 140 (4) (1993) 1018–1026.
[4] P. Allongue, Phys. Rev. Lett. 77 (10) (1996) 1986–1989.
[5] M.A. Gosálvez, A.S. Foster, R.M. Nieminen, Europhys. Lett., 2002, in press.
[6] G.F. Cerofolini, L. Meda, Appl. Surf. Sci. 89 (1995) 351–360.
[7] A.J. Pietsch, G.S. Higashi, Y.J. Chabal, Appl. Phys. Lett. 64 (23) (1994) 3115.
[8] M.A. Gosálvez, R.M. Nieminen, P. Kilpinen, E. Haimi, V. Lindroos, Appl. Surf. Sci. 178 (2001) 7–26.
[9] M.A. Gosálvez, R.M. Nieminen, in preparation.
[10] H. Camon, Z. Moktadir, M. Djafari-Rouhani, Mater. Sci. Eng. B 37 (1996) 142–145.
[11] Z. Zhu, C. Liu, Comput. Model. Eng. Sci. 1 (1) (2000) 11–19.
[12] G. te Velde, J. Comp. Chem. 22 (2001) 931.
[13] A.D. Becke, Phys. Rev. A 38 (1988) 3098.
[14] C. Lee, W. Yang, R.G. Parr, Phys. Rev. B 37 (1988) 785.
[15] M.K. Weldon, B.B. Stefanov, K. Raghavachari, Y.J. Chabal, Phys. Rev. Lett. 79 (1997) 2851.
[16] A. Vittadini, A. Selloni, M. Casarin, Phys. Rev. B 52 (1995) 5885.
[17] H. Ibach, H. Wagner, D. Bruchmann, Solid State Commun. 42 (1982) 457.
[18] M. Shikida, K. Sato, K. Tokoro, D. Uchikawa, Sens. Actuators A 80 (2000) 179–188.
[19] P.H. Chen, H.Y. Peng, C.M. Hsieh, M.K. Chyu, Sens. Actuators A 93 (2001) 132–137.
[20] I. Zubel, Sens. Actuators A 70 (1998) 260–268.
[21] I. Zubel, Sens. Actuators A 94 (2001) 76–86.
[22] I. Zubal, I. Barycka, K. Kotowska, M. Kramkowska, Sens. Actuators A 87 (2001) 163–171.
[23] R.J. Jaccodine, J. Appl. Phys. 33 (1962) 2643–2647.
[24] D.W. Shaw, J. Crystal Growth 47 (1979) 509–517.
[25] B. Puers, W. Sansen, Sens. Actuators, A: Phys. A21–A23 (1990) 1036–1041.
[26] H. Seidel, L. Csepregi, A. Heuberger, H. Baumgartel, J. Electrochem. Soc. 137 (1990) 3612–3626.
[27] H. Schröder, E. Obermeier, J. Micromech. Microeng. 10 (2000) 163–170.